Int Ophthalmol (2024) 44:267
https://doi.org/10.1007/s10792-024-03196-5

ORIGINAL PAPER

Morphometric evaluation of the anatomical relationships between the superior orbital fissure and the orbital structures based on computed tomography images with clinical implications

Esin Erbek · Aynur Emine Çiçekcibaşı · Gülay Açar · Betül Digilli Ayaş · Demet Aydoğdu

Received: 6 February 2024 / Accepted: 15 June 2024

Abstract

Purpose To assist in surgical planning in endoscopic approaches, we analyzed the morphometric measurements of the superior orbital fissure (SOF) and optic canal (OC) by three-dimensional multislice computed tomography (3D MDCT) and evaluated them according to age, gender, and lateralization.

Methods The study analyzed 219 MDCT images (114 women, 105 men) from individuals aged 18–90. Measurements of SOF and OC were performed on 3D MDCT images in the axial plane and with 3D-Slicer software.

Results The distance between the infraorbital foramen and the anterior entrance of the maxillary sinus (CBW) ($p<0.001$), the distance between the CBW and the lateral point of the SOF ($p=0.001$), and the Angle 1 ($p=0.028$) were higher in women than in men. While the SOF length and on 3D the SOF width were higher in women than men ($p<0.001$ and ($p=0.001$, respectively), the lateral wall length OC was higher in men than women ($p=0.045$). According to SOF classification, SOF length was highest in type II and lowest in type VIII ($p=0.025$), SOF width was highest in type I and lowest in type VI ($p<0.001$). No significant difference was found based on age groups and lateralization in all parameters.

Conclusion We found that as the SOF width increased, the SOF length also increased, and there was a statistically strong positive correlation. These findings can contribute to a more effective and safe operation by improving and updating surgeons' knowledge about safe distances to SOF in endoscopic procedures from a 3D MDCT perspective.

Keywords Superior orbital fissure · Optic canal · Morphometry · Morphology · Computed tomography

E. Erbek (✉) · A. E. Çiçekcibaşı · G. Açar · B. Digilli Ayaş
Department of Anatomy, Faculty of Medicine, Necmettin Erbakan University, 42090 Meram, Konya, Turkey
e-mail: esinerbek89@gmail.com

A. E. Çiçekcibaşı
e-mail: aynurcicekcibasi@yahoo.com.tr

G. Açar
e-mail: gulayzeynep73@gmail.com

B. Digilli Ayaş
e-mail: betuldigilli@gmail.com

D. Aydoğdu
Department of Radiology, Faculty of Medicine, Necmettin Erbakan University, 42090 Meram, Konya, Turkey
e-mail: drdemet25@hotmail.com

Introduction

The orbit is best described as a pyramid with a conical or quadrangular base. The anterior part of this pyramid is its base, formed by the orbital rim, and its narrowest segment is the orbital apex, located posteriorly [1]. The orbital apex is the area between the orbit and the intracranial space,

Published online: 24 June 2024

containing structures such as the optic canal (OC), superior orbital fissure (SOF), and inferior orbital fissure [2]. The SOF is a small and topographically significant area connecting the middle cranial fossa to the orbit. The SOF is a three-dimensional space with a highly variable shape, located lateral to and below the OC, bounded medially by the lesser wing of the sphenoid, inferiorly and laterally by the greater wing of the sphenoid, and superiorly by the frontal bone. The SOF is divided into two parts: the superior-lateral part, which includes the trochlear, lacrimal, frontal nerves and the superior ophthalmic vein, and the inferior-medial part, which consists of the superior and inferior branches of the oculomotor nerve, nasociliary nerve, abducens nerve, sensory and sympathetic root of the ciliary ganglion [3]. The lesser wing of the sphenoid arises from the lateral aspect of the body of the sphenoid bone, anteriorly and superiorly, as two roots. Between these two roots is the OC, which connects the orbit to the middle cranial fossa [4]. It contains the optic nerve, dura mater, arachnoid mater, ophthalmic artery, and sympathetic nerves [5]. The contents of the SOF and the OC are the most likely structures to be affected by pathology at the apex [1].

Traditional surgical approaches to the orbit and orbital apex include lateral and medial orbitotomy and transcranial approaches. These approaches are highly invasive, with a high morbidity rate, and can be devastating. With the introduction of functional endoscopic sinus surgery in the 1980s, endoscopic techniques and approaches were developed to diagnose and treat inflammatory and benign lesions of the nasal and paranasal sinuses. The endoscopic endonasal approaches for the orbit were considered practical alternatives for selected pathologic lesions of this region, even advantageous over some transcranial and transorbital approaches. The endoscopic endonasal approach to the orbital apex and wall is increasingly used [6]. The optic nerve's anatomical position is paramount for any procedure accessing the SOF and the intraconal space. The optic nerve is lateral to the SOF when accessed through the endoscopic endonasal approaches; therefore, it is protected as long as one does not surpass the boundaries of the SOF [7].

The transmaxillary approach, directed from the orbital floor, is most commonly performed with endoscopic assistance using a sublabial incision in the gingivobuccal margin [8]. This approach is less invasive than the transcranial approach and gives cosmetically more acceptable results than other approaches to the orbit; it is applicable not only for the excision of intraorbital tumors but also for different uses, such as orbit decompression [9]. The endoscopic sublabial transmaxillary approach has been reported to provide safe and direct access to the rostral middle fossa, eliminating the need for brain retraction and external incisions and allowing early devascularization of cranial or dural-based lesions [10]. Additionally, it has been noted that the transmaxillary approach can visualize inferior intraconal structures without risking the infraorbital nerve and artery and that the optic nerve can be more easily visualized with the approach medial to the inferior rectus muscle [11]. Wang et al. [12] reported in their study that the endoscopic transmaxillary approach provided adequate endoscopic visualization and reliable decompression of the SOF, eliminating the need for brain retraction, temporal muscle manipulation, or any external incision, and resulted in functional improvement.

In previous studies, safe distance and morphometric measurements were performed on cadavers in endoscopic approaches to the orbit [7, 12–17]. The distinctive aspect of our research is that we measured the safe distances and morphometric measurements used in endoscopic approaches to the SOF and OC on 3D-CT images.

While partial investigations have been conducted on the dimensions, variations, and anatomical landmarks of SOF and OC used in surgical interventions such as endoscopic endonasal approaches in various studies, as far as we know, there is currently no comprehensive study in the accessible literature that extensively examines these structures using three-dimensional computed tomography (3D-CT). Therefore, we aimed to thoroughly investigate the detailed anatomical features of the SOF and OC using 3D-CT, considering age, lateralization and gender differences. We aimed that our collected data can contribute to the existing body of knowledge, help prevent potential complications in surgical interventions, and facilitate radiological evaluations.

Materials and methods

Approval statement of the study

Necmettin Erbakan University Faculty of Medicine institutional ethics review board approved the present study (Approval protocol number: 2021/3391).

Subjects

In this study, the authors retrospectively analyzed the paranasal and orbital MDCT images of 219 patients (114 women and 105 men) between the ages of 18 and 90 years enrolled between January 2018 and May 2021 with various indications. Only individuals without any pathology and surgical history in the region were included in the study, and those under 18 years of age, with pathologies such as tumors or fractures in bony structures including the orbit, history of surgery in the region, and those with CT image artifacts were excluded from the study.

Study design

The scan parameters of all CT images obtained using the 256-slice Multidetector CT Somatom Drive (Siemens Healthineers, Germany) scanner are as follows: slice thickness 0.625 mm; field of view (FOV) 220 mm; exposure 120 kV, 74 mA, 60 mAs; rotation time 0.28 s. Images obtained in DICOM format were uploaded to 3D-Slicer, an open-source software platform, and displayed in axial section and 3D images with the help of multiplanar reconstruction. An experienced radiologist and two anatomists decided on the eligibility of CT images to include in this study.

Morphometric measurements

Based on data provided by Reymond et al. [18], Wang et al. [12], and Nitek et al. [19], all reformatted images were used to measure these surgical morphometric parameters from each side and gender discrimination.

The measurements were made on axial and three-dimensional MDCT images, and Table 1 summarizes all the measurements, along with their explanations. The distances from the OC to the medial point of the SOF (a), the midpoint between the lateral and medial edges of the SOF (b) and the lateral point of the SOF (c) were measured (Fig. 1). The distance from the center of the bone window (CBW) on the anterior wall of the maxillary antrum to the anterior nasal spine (ANS) and infraorbital foramen (IF) (Fig. 2a), the distance from the CBW to the most lateral point on the lateral wall of the superior orbital fissure (MLS) and the most medial point on the lateral wall of the superior orbital fissure (MMS) (Fig. 2b), and the distance from the entry point of the infraorbital sulcus (EIS) into the orbit to the MLS and MMS (Fig. 2c) were measured as shown in Fig. 2. Angle 1 (Fig. 3a) between CBW-MLS line and CBW-MMS line and Angle 2 (Fig. 3b) between EIS-MLS line and EIS-MMS line were evaluated and are illustrated in Fig. 3. The longest distance between the corners of the structure was measured for the SOF length (Fig. 4a), the largest distance between the medial and lateral walls was measured for the SOF width (Fig. 4b)**.** Morphological classification of the SOF by shapes were evaluated on 3D-CT images and classified according to Reymond et al. [18]. In this study, nine morphological types of SOF were observed, ranging from a shape with a noticeable constriction to a gradually increasing width. The shape of SOF was analyzed by nine basic morphological types (I–IX) and shown in Fig. 5. Also, the distance from the frontozygomatic (FZ) suture to the lateral edge of the OC (Fig. 6a) and the distance from the anterior lacrimal crest (ALC) to the medial border of the OC (Fig. 6b) were measured.

Based on data provided by Hart et al. [20], Kalthur et al. [21], Gosavi et al. [22], and Park and Kim [23], all reformatted images were used to measure these morphometric parameters from each side and gender discrimination. SOF width (Fig. 7a) and OC widths, which are the anterior of the orbital opening and the posterior of the cranial opening (Fig. 7b) were measured in the axial plane. Also, the medial and lateral wall lengths of the optic canal formed by the sphenoethmoidal cell of the posterior ethmoid sinus medially and the sphenoid sinus; and the anterior clinoid process laterally were measured in the axial plane and depicted in Fig. 7c.

Statistical analysis

All these statistical analyses were performed with the SPSS (Statistical Package for the Social

Table 1 Definitions of measurements

Measurements	Definitions
3D-CT parameters	
a (mm)	Distance from the OC to the medial point of the SOF.
b (mm)	Distance from the OC to the midpoint between the lateral and medial edges of the SOF.
c (mm)	Distance from the OC to the lateral point of the SOF.
CBW-ANS (mm)	The distance from the center of the bone window (CBW) on the anterior wall of the maxillary antrum to the anterior nasal spine (ANS).
CBW-IF (mm)	The distance from the center of the bone window (CBW) on the anterior wall of the maxillary antrum to the infraorbital foramen (IF).
CBW-MLS (mm)	The distance from the CBW to the most lateral point on the lateral wall of the SOF (MLS).
CBW-MMS (mm)	The distance from the CBW to the most medial point on the lateral wall of the SOF (MMS).
EIS-MLS (mm)	The distance from the entry point of the infraorbital sulcus (EIS) to the most lateral point on the lateral wall of the SOF (MLS).
EIS-MMS (mm)	The distance from the entry point of the infraorbital sulcus (EIS) to the most lateral point on the medial wall of the SOF (MMS).
Angle 1 (º)	The angle between the CBW-MLS line and the CBW-MMS line.
Angle 2 (º)	The angle between the EIS-MLS line and the EIS-MMS line.
SOF length (mm)	The longest distance between the corners.
SOF width3D (mm)	The largest distance between the medial and lateral walls.
OC-FZ (mm)	The distance from the frontozygomatic (FZ) suture to the lateral edge of the OC.
OC-ALC (mm)	The distance from the anterior lacrimal crest (ALC) to the medial border of the OC.
Axial parameters	
SOF width (mm)	The width of the superior orbital fissure (SOF) in the horizontal plane, including the optic canal (OC).
Orbital width of OC (mm)	The width of the orbital opening.
Intracranial width of OC (mm)	The width of the cranial opening.
Medial wall length of OC (mm)	The length of the canal formed medially by the sphenoethmoidal cell of the posterior ethmoid sinus and the sphenoid sinus.
Lateral wall length of OC (mm)	The length of the canal formed laterally by the anterior clinoid process.

Sciences) software version 28.0 program. The mean ± standard deviation (SD) for numeric variables as descriptive data and percentages for categorical variables were presented. Compliance of morphometric parameters with normal distribution was evaluated with the Kolmogorov–Smirnov test. Student's t-test and paired t-test were used to compare the differences between genders and laterality, respectively. One-way analysis of variance (ANOVA) was used for comparison in more than two independent groups. In addition, Pearson's correlation coefficient was used to evaluate the relationships among numerical variables. Differences in categorical variables were assessed using the Chi-square test. A value of $p < 0.05$ was noted as statistically significant.

Results

Among the 219 patients (range 20–73 years, mean age 41.95 ± 13.04 years) in this retrospective investigation, 114 were females (mean age 41.07 ± 13.93 years) and 105 males (mean age 42.90 ± 11.96 years). Patients were divided into three age groups as follows: 80 (36.5%) Group I (20–34 years); 76 (34.7%) Group II (35–49 years); 63 (28.8%) Group III (50–73 years).

Morphometric measurements were analyzed according to gender and laterality. No significant difference was detected between the right and left sides for all distances measured. Additionally, CBW-IF ($p < 0.001$), CBW-MLS ($p = 0.001$), Angle 1 ($p = 0.028$), SOF length ($p < 0.001$), and SOF width3D ($p = 0.001$) were significantly higher in

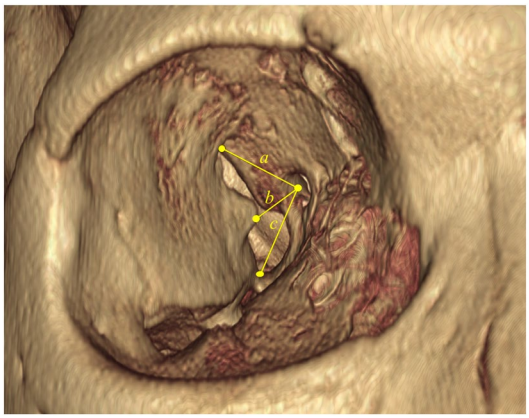

Fig. 1 Three-dimensional (3D) reconstruction computed tomography (CT) images. The distances between optic canal (OC) and superior orbital fissure (SOF) was showed with yellow line on the right side of the orbit. The distance from the lateral margin of OC to the medial pole of SOF (**a**), the distance from the lateral edge of the OC to the midpoint of the fissure (**b**), the distance from the lateral margin of OC to the lateral pole of SOF (**c**)

females than males (Table 2). This result suggests gender-related differences in the SOF length and width anatomy. The distance from OC to FZ was 49.51 mm in men and 48.98 mm in women ($p=0.179$), and the distance from OC to ALC was 44.98 mm in men and 44.70 mm in women, respectively ($p=0.478$).

The orbital width of the OC was 3.50 mm in men and 3.28 mm in women ($p=0.132$), while the intracranial width of the OC was 7.52 mm in men and 7.44 mm in women ($p=0.654$). The mean value of the medial wall length of the OC in men was 7.59 mm, while this value was 7.05 mm in women ($p=0.097$). The mean value of the lateral wall length of OC in men was 9.08 mm, while this value was 8.56 mm in women ($p=0.045$). (Table 2).

In the statistical analysis of the morphometric data obtained according to the morphological types of the SOF, while SOF length was significantly highest in Type II and lowest in Type VIII ($p=0.025$), SOF width was significantly highest in Type I and lowest in Type VI ($p<0.001$). Other morphometric measurements didn't show any statistical significance according to the morphological types of the SOF (Fig. 8).

No significant differences were found in the statistical analysis of morphometric data according to age groups. Additionally, when gender and age groups were compared according to the SOF types, no statistically significant difference was observed. The correlation analysis showed that SOF and OC were not associated with age. A strong positive correlation was seen between the lateral and medial walls of the OC length, while a significant and strong negative correlation was observed between the orbital and intracranial width of the OC. There was a strong positive correlation between SOF width3D and SOF length.

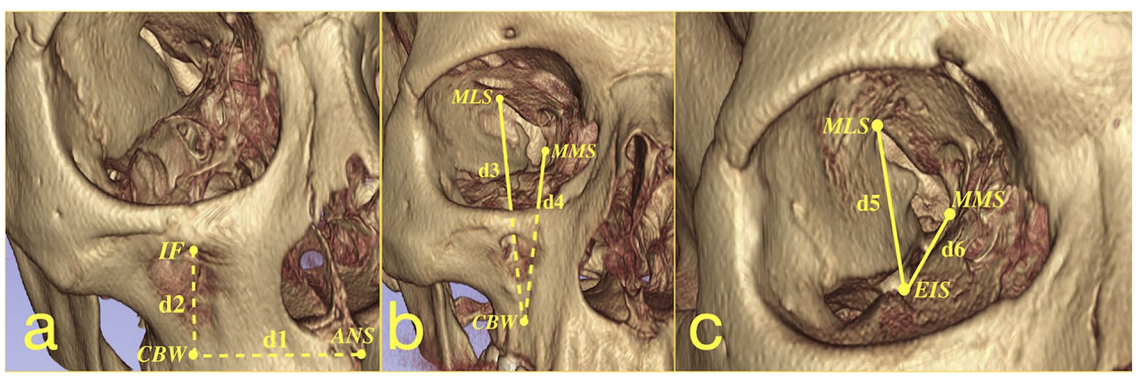

Fig. 2 Three-dimensional (3D) reconstruction computed tomography (CT) images. **a** The distance from the center of the bone window (CBW) to the anterior nasal spine (ANS) (d1) and the distance from CBW to the infraorbital foramen (IF) (d2). **b** The distance from CBW to the most lateral point in the lateral wall of superior orbital fissure (MLS) (d3) and the distance from CBW to the most medial point in the lateral wall of superior orbital fissure (MMS) (d4). **c** The distance from the entering point of the infraorbital sulcus (EIS) to MLS (d5) and the distance from EIS to MMS (d6)

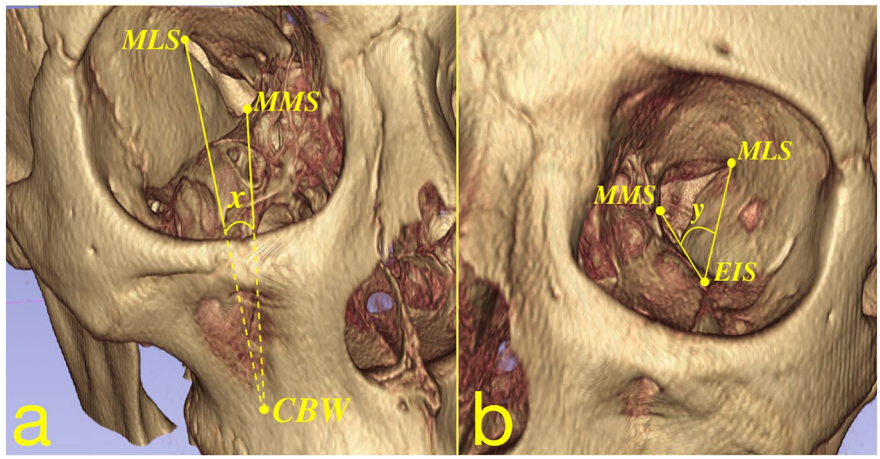

Fig. 3 Three-dimensional (3D) reconstruction computed tomography (CT) images. **a** Angle 1 (*x*), the angle between the lines (CBW-MLS and CBW-MMS) from the center of the bone window (CBW) to the most lateral point in the lateral wall of superior orbital fissure (MLS) and the most medial point in the lateral wall of superior orbital fissure (MMS) **b** Angle 2 (*y*), the angle between the lines (EIS-MLS and EIS-MMS) from the entering point of the infraorbital sulcus (EIS) to MLS and MMS

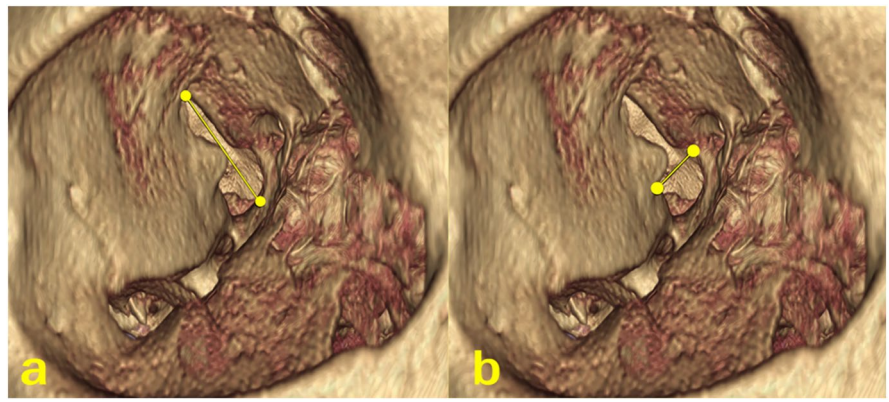

Fig. 4 Three-dimensional (3D) reconstruction computed tomography (CT) images of the right side of the orbit. **a** Superior orbital fissure (SOF) length was showed with yellow line. **b** SOF width was showed with yellow line

Discussion

Neurosurgical approaches, such as the fronto-orbito-zygomatic cranio-orbitotomy, can provide a global view of the deep and medial components of the orbit, including the orbital apex, the OC, and adjacent intracranial structures. More recently, endoscopic approaches to the orbit have been developed and described in the surgical treatment of extraconal, particularly for the orbital apex and periorbital skull base, as well as intraconal lesions. Several studies have shown similar efficacy and complication rates compared to traditional external approaches [24].

The experience with the endoscopic approach to pathologic lesions in the orbital apex has demonstrated the advantages of this approach to this region. The fast advancement of endonasal endoscopic techniques for approaching the orbit has standardized their use for some pathologic lesions [6]. The SOF and its critical relationships have been inadequately described from an endoscopic endonasal perspective, and many previous papers have emphasized the microsurgical anatomy of the SOF, thereby increasing interest in this area. Most authors concur that only the medial aspect of the SOF is functionally relevant, as no major neural and vascular structures pass through the lateral compartment.

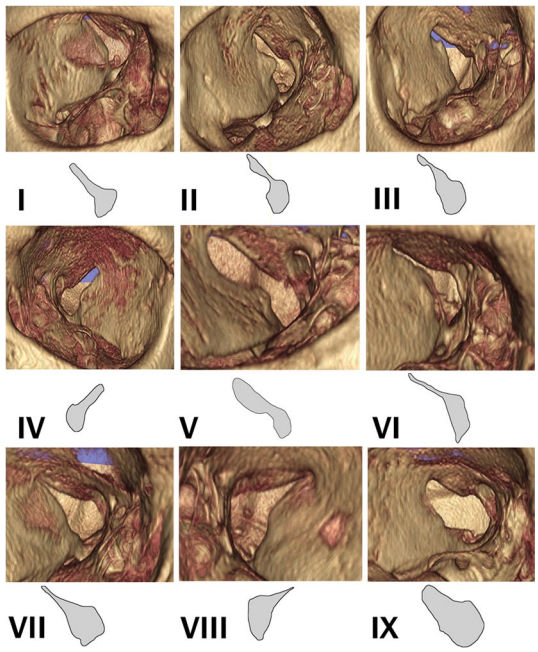

Fig. 5 Three-dimensional (3D) reconstruction computed tomography (CT) images. The morphological types of the SOF (I-IX) was showed with schematic drawings and 3D reconstruction CT images

This information highlights the potential role of endoscopic endonasal approaches compared to traditional neurosurgical approaches in addressing these critical areas [16].

The anatomical position of the optic nerve is crucial for any procedure accessing the SOF and the intraconal space. When accessed through the endoscopic endonasal approach, the optic nerve lies lateral to the SOF; hence, it remains protected as long as the boundaries of the SOF are not exceeded. Conversely, when dealing with lesions originating in the superolateral orbit via a transorbital approach, the optic nerve is situated in the dorsoventral aspect and is at risk [7]. Abed et al. [1] reported that in a study on 24 cadavers, the mean distance from the midpoint of OC to the tip of SOF was 10.22 mm. In a study on 100 cadavers, the mean values of the distances between the lateral, middle, and medial points of the OC and SOF were measured as 16.84 mm, 9.28 mm and 10.88 mm, respectively [18]. In our study, a total of 438 orbit 3D-CT images were analyzed, and the distances between the medial, midpoint, and lateral endpoint of the OC and SOF were measured as 16.73 mm, 9.77 mm and 11.37 mm in men and 17.16 mm, 10.02 mm and 11.49 mm in women, respectively. The findings obtained could be utilized to plan a safe surgical approach based on the specific goals of the orbital procedure being performed. This technique can potentially be adapted and implemented for various surgical approaches. With limited comparative studies on 3D CT images and sample size available in the literature, our research findings hold significant value. Therefore, our study could contribute value to surgeons' preoperative planning efforts.

The transmaxillary approach to the orbit offers suitable direct access to the inferior orbital region within a short operative time range and without a craniotomy, orbitotomy, and related complications. The surgical technique of the transmaxillary approach is anatomically divided into two steps: Caldwell-Luc operation, opening the inferior wall of the eye, and removal of the tumor. Caldwell-Luc operation is technically simple and safe. The complications of this operation are limited. Rarely, infraorbital nerve and dental injury, recurrent maxillary sinus infections,

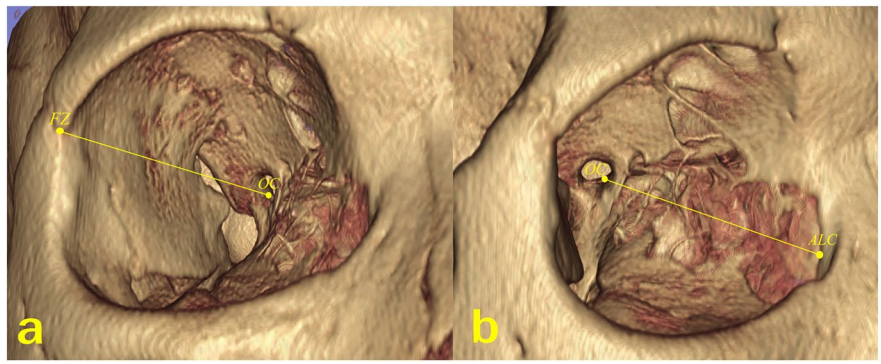

Fig. 6 Three-dimensional (3D) reconstruction computed tomography (CT) images. **a** The distance between the frontozygomatic (FZ) suture and the optic canal (OC) was showed with yellow line. **b** The distance between the anterior lacrimal crest (ALC) and OC was showed with yellow line

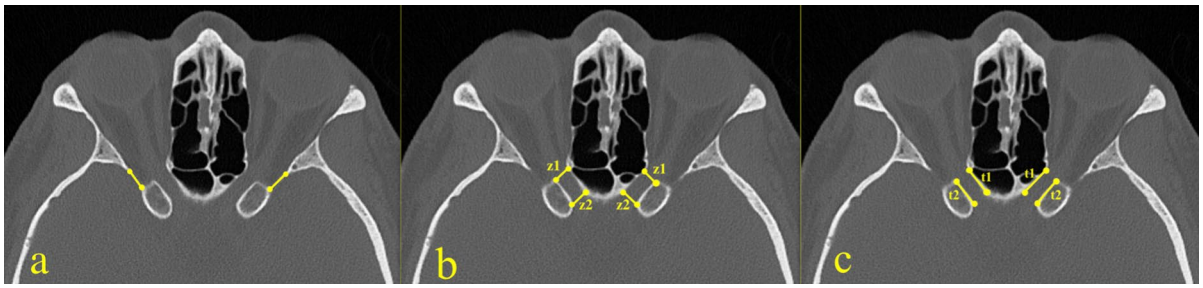

Fig. 7 Axial CT images**. a** Widths of the superior orbital fissure were shown with yellow lines on both sides**. b** Widths of the optic canal's (OC) orbital (z1) and intracranial (z2) parts were shown with yellow lines for both sides**. c** Medial (t1) and lateral (t2) wall lengths of OC were shown with yellow lines for both sides

Table 2 Statistical analysis of morphometric parameters by gender

Measurements	Male ($n=105$) Mean ± SD	Female ($n=114$) Mean ± SD	*p-value*
3D-CT parameters			
a (mm)	16.73 ± 3.64	17.16 ± 3.13	.181
b (mm)	9.77 ± 2.32	10.02 ± 2.03	.232
c (mm)	11.37 ± 1.69	11.49 ± 1.72	.454
CBW-ANS (mm)	29.81 ± 4.22	29.37 ± 4.24	.275
CBW-IF (mm)	17.18 ± 4.08	18.98 ± 3.70	**< 0.001***
CBW-MLS (mm)	56.26 ± 5.23	57.88 ± 4.83	**.001***
CBW-MMS (mm)	50.81 ± 5.67	51.58 ± 5.20	.139
EIS-MLS (mm)	23.61 ± 3.37	23.33 ± 2.76	.337
EIS-MMS (mm)	24.35 ± 3.26	24.13 ± 3.06	.459
Angle 1 (°)	19.66 ± 4.02	20.48 ± 3.76	**.028***
Angle 2 (°)	43.82 ± 8.12	44.88 ± 8.59	.183
SOF length (mm)	18.54 ± 3.88	20.72 ± 2.28	**< 0.001***
SOF width3D (mm)	7.02 ± 1.88	7.57 ± 1.48	**.001***
OC-FZ (mm)	49.51 ± 3.74	48.98 ± 4.45	.179
OC-ALC (mm)	44.98 ± 4.36	44.70 ± 3.75	.478
Axial parameters			
SOF width (mm)	6.22 ± 2.02	6.38 ± 2.02	.404
Orbital width of OC (mm)	3.50 ± 1.50	3.28 ± 1.54	.132
Intracranial width of OC (mm)	7.52 ± 1.82	7.44 ± 1.91	.654
Medial wall length of OC (mm)	7.59 ± 3.45	7.05 ± 3.35	.097
Lateral wall length of OC (mm)	9.08 ± 2.75	8.56 ± 2.67	**.045***

p values in bold indicate significant values ($p < 0.05$)

SOF width: width of superior orbital fissure, SOF width3D width of superior orbital fissure on the 3D-CT image, SOF length length of superior orbital fissure, 'a' distance between the medial margin of the SOF and the lateral margin of the OC, 'b' distance between the midpoint of the SOF and the lateral margin of the OC, 'c' distance between the lateral margin of the SOF and the lateral margin of the OC, CBW-IF distance between centre of bone window in the anterior wall of maxillary antrum and infraorbital foramen, CBW-ANS distance between centre of bone window in the anterior wall of maxillary antrum and anterior nasal spine, CBW-MMS distance between centre of bone window in the anterior wall of maxillary antrum and most medial point of SOF, CBW-MLS distance between centre of bone window in the anterior wall of maxillary antrum and most lateral point of SOF, EIS-MMS distance between entering point of the infraorbital sulcus in the orbit and most medial point of SOF, EIS-MLS distance between entering point of the infraorbital sulcus in the orbit and most lateral point of SOF, the Angle 1 between the CBW-MLS line and the CBW-MMS line; the Angle 2 between the EIS-MLS line and the EIS-MMS line. OC optic canal, OC-FZ distance between optic canal and frontozygomatic suture, OC-ALC distance between optic canal and anterior lacrimal crest, SD standard deviation, *n* sample size *Statistically significant *p* value ($p < 0.05$)

ecchymosis, and cheek edema can be seen. The transmaxillary route provides excellent exposure of the optic, oculomotor, ciliary nerves, ciliary ganglion, retinal and ciliary posterior arteries, ocular muscles, orbit's fat tissue, and other vital structures. So, the incidence of complications related to exposure to these structures may be reduced [25]. In a cadaveric study of the transmaxillary endoscopic approach to the orbit, the CBW anatomical point in the canine fossa on both sides of the face was utilized. The study found that inserting the endoscope into the maxillary sinus allowed for easy penetration, identification of the infraorbital canal, which is the exit point of the infraorbital nerve, and determination of the nerve branches [11]. In another study, the CBW point was employed for the surgical approach to the maxillary sinus. The study concluded that this anatomical point provides easy and safe access to the orbit and direct access to the middle cranial fossa [10].

A study conducted on ten cadavers examined transmaxillary transmüller muscle decompression of SOF and its clinical application on a patient with posttraumatic superior orbital fissure syndrome (SOFS) [12]. The study measured distances from the CBW point to the IF and the ANS as 14.9 mm and 32.1 mm and from the CBW point to the SOF medial and lateral points as 49.4 mm and 53.2 mm, respectively. Additionally, the mean distances from the infraorbital foramen entry point to the SOF's medial and lateral points were 13.1 mm and 15.4 mm, respectively. In our research, we observed that women demonstrated higher CBW-IF and CBW-MLS values than men, surpassing the results reported in a previous study [12]. Furthermore, our study included specific measurements of EIS-MMS, EIS-MLS, and Angle 2, a departure from the existing literature. Moreover, a smaller Angle 1 allows for direct access to the lateral wall of the SOF while minimizing the retraction of orbital structures [12]. In our study, Angle 1 was significantly lower, with 19.66º in men and 20.48º in women ($p=0.028$). We anticipate that the findings from the study employing 3D-CT will be advantageous for achieving safe and easy proximity to the SOF. Also, the utilization of Angle 1 in navigating the approach to the lateral wall of the SOF will serve as a valuable reference for surgeons planning an endoscopic transmaxillary approach to this area. In addition, studies in the literature have been conducted on cadavers, but there is a lack of an adequate number of studies performed on 3D-CT scans for comparison. Therefore, our study is essential as it provides measurements of CBW and EIS points on 3D-CT images for the transmaxillary approach and offers a different perspective for future studies. Specifically, we believe that our study will contribute to the literature due to its substantial sample size of 438 orbits.

The limited size of the SOF could decrease the ability of nerves to withstand direct pressure and swelling. Any swelling following surgery could compress the nerves and hinder blood flow, leading to SOFS. Either traumatic or non-traumatic causes can bring it about. In cases of traumatic injury, fractured bones and hematoma directly apply pressure on the nerves, and subsequent infection and swelling disrupt the blood flow around the SOF, resulting in SOFS [26]. Some authors suggested that a congenitally narrow SOF (less than 1.60 mm) is a risk factor for the SOFS [23, 26–29]. The comparison of the studies on the SOF length and width was summarized in Table 3. The distance from the superomedial edge to the superolateral edge of the SOF was measured as 15.9 mm by Natori et al. [30] and 16.9 mm by Govsa et al. [27]. A study comparing the width of SOF in CT scans and cadavers found that the width of SOF was 3.73 ± 1.64 mm in CT scans and 3.21 ± 1.09 mm in cadavers. In this study, it was observed that there was no significant difference between the width of CT scans and cadavers [26]. In their research, Reymond et al. [18] measured the maximum lengths and widths of the SOFs in 100 adult cadaver skulls. They categorized the fissures into type "a" with significant narrowing and type "b" without such narrowing. Type "a" had the SOF width of 7.31 mm and SOF length of 17.47 mm, while type "b" had the SOF width of 7.86 mm and the SOF length of 12.48 mm. Besides, they found that the lengths of type "a" and "b" fissures were different, with type "b" being significantly shorter. A different research study utilized 3D-CT scanning to assess the dimensions of the SOF across eight age categories, spanning from infants to individuals over 60 years old. The results indicated that the average length of the SOF measured 16 ± 2.3 mm on the right side and 15.8 ± 2.2 mm on the left side, with an average width of 6.3 ± 1.3 mm on the right side and 6.4 ± 1.3 mm on the left side [31]. In our research, while the SOF length was 19.67 mm on the right side and 19.68 mm on the left side, SOF width was 7.28 mm on the right side and 7.34 mm on the

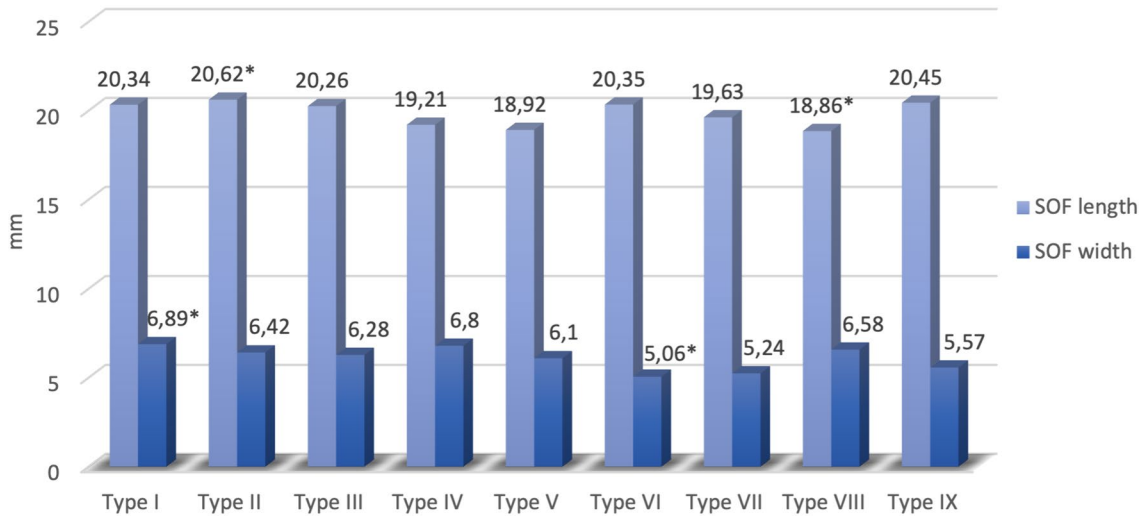

Fig. 8 The mean values of superior orbital fissure (SOF) lengths and widths according to the types of SOF. *Statistically significant *p* value ($p < 0.05$)

Table 3 Comparison of superior orbital fissure width and length with some previous studies

Study	*N*	Method	SOF length Mean ± SD (mm)	SOF width Mean ± SD (mm)
Reymond et al. [18]	100	Cadaver	Type a: 17.47 Type b: 12.48	Type a: 7.31 Type b: 7.86
Patel et al. [33]	30	Dry skulls, CT	D: 15.93 ± 3.41 CT: 10.90 ± 1.20 D: 16.18 ± 2.89 CT: 10.92 ± 1.25	D: 8.64 ± 1.42 CT: 6.14 ± 0.95 D: 8.44 ± 1.27 CT: 6.13 ± 1.18
Park et al. [23]	142	CT	–	R-M: 3.78 ± 0.92 L-M: 3.79 ± 0.96 R-F: 3.69 ± 1.18 L-F: 3.62 ± 1.34
Fujiwara et al. [26]	32	Cadaver, CT	–	C: 3.16 ± 1.24 CT: 3.61 ± 1.70 C: 3.27 ± 1.05 CT: 3.87 ± 1.60
Pirinc et al. [31]	200	3D-MDCT	R-M: 15.9 ± 0.24 R-F: 16.1 ± 0.23 L-M: 15.8 ± 0.24 L-F: 15.8 ± 0.21	R-M: 6.1 ± 0.13 R-F: 6.5 ± 0.13 L-M: 6.2 ± 0.14 L-F :6.5 ± 0.11
The present study	219	3D-MDCT, CT	M: 18.54 ± 3.88 F: 20.72 ± 2.28 R: 19.67 ± 3.24 L: 19.68 ± 3.42	CT-M: 6.22 ± 2.02 CT-F: 6.38 ± 2.02 CT-R: 6.25 ± 2 CT-L: 6.25 ± 2 3D-CT-M: 7.02 ± 1.88 3D-CT-F: 7.57 ± 1.48 3D-CT-R: 7.34 ± 1.72 3DCT-L: 7.34 ± 1.72

SOF Superior orbital fissure, *C* Cadaver, *CT* Computed tomography, *D* Dry skulls, *3D-MDCT* Three dimensional multidedector computed tomography, *N* Subjects, *M* Male, *F* Female, *R* Right, *L* Left, *SD*-Standard Deviation

left side on 3D-CT images. The SOF width measured in axial images was found to be 6.26 mm on the right and 6.25 mm on the left. Additionally, the mean values of SOF width measured on axial CT were lower than those measured on 3D CT. The current study did not show any statistically significant difference between the two sides, which was consistent with the results of previous studies [26, 32, 33].

The SOF is wider medially with a long axis sloping infero-medially and forwards. The orbital apex is at the medial and lower end of the SOF where it is widest, extends obliquely in the lateral direction, and forwards between the roof and lateral wall of the orbit. It was observed in different shapes varying from an oblique cleft, roughly triangular, to a club-shaped or slit-like opening in the middle cranial fossa. Various shapes of SOF, as described by Sharma et al. [34], are shown. Shapiro and Janzen (1960) were the first to classify the shape of the SOF and described six different shapes [27]. Sharma et al. [34] supplemented this classification with three additional shapes. Magden et al. [35] introduced one more shape to the classification initially proposed by Sharma et al. [34], resulting in nine different shapes. In the literature, studies have classified the SOF into nine different shapes [18, 27, 29]. One study noted that the most common shape was bilateral Type VI, followed by Type VIII on the right and Type III on the left [29].

Moreover, another study reported varying incidence rates of fissure types in both right and left-sided SOFs, with triangular, classical, oval, and irregular fissures observed, each with different prevalence rates on either side [36]. In the study conducted on 3D-CT images, seven different types of SOF were identified: curved, flat, racket-shaped, eight-shaped, key-shaped, narrow, and triangular types [31]. Govsa et al. [27] classified SOF types, noting Type VI as the most common, observed in 35.4% of cases. In our study, SOF was observed in nine different shapes ranging from Type I to Type XI, with variations in width. SOF length ranged from highest in Type II to lowest in Type VIII. SOF width varied significantly, being widest in Type I and narrowest in Type VI. These results highlight the importance of fissures not only in shape but also in area. A strong positive correlation was found between SOF width3D and SOF length, but no significant correlation was found between SOF length and age. It was determined in this study that as the width of the SOF increased, the length of the SOF also increased, indicating a statistically strong positive relationship. The findings of Reymond et al. [18] support our study and once again emphasize that a short fissure does not necessarily imply width, nor does a long fissure imply narrowness.

The optic nerve may face compression due to direct or indirect maxillofacial injuries, fibrous dysplasia, osteopetrosis, and tumors in the region. Optic nerve decompression becomes necessary in such cases, where the OC can be accessed through trans-ethmoidal, trans-sphenoidal, or supraorbital routes [37]. The OC, situated at the orbital apex, serves as the narrowest point, allowing passage of the optic nerve from the orbit to the middle cranial fossa. Precise knowledge of its dimensions on both sides, in men and women, and across different populations is essential for evaluating and managing various optic neuropathies. Recent advancements in endoscopic endonasal optic nerve decompression, as well as other surgical approaches to the optic nerve like transfrontal craniotomy, orbitotomy, and trans-ethmoidal and spheno-ethmoidal surgeries, underscore the importance of accurate understanding of the morphological and metric details of the OC specific to each population [38]. Consequently, numerous studies have delved into the microsurgical anatomy of the OC, aiming to identify critical points during optic nerve decompression and develop techniques for exposing the OC [5, 39].

Morphometric measurements of the OC hold great significance as it serves as a connection between the intracranial cerebrospinal fluid space and the subarachnoid space of the intraorbital portion of the optic nerve, with the narrowest subarachnoid space size. This connection underscores the potential role of impaired cerebrospinal fluid circulation in conditions like normal-tension glaucoma and papilledema [38]. Previous studies about OC measurements are summarized in Table 4. In a study conducted on 50 dry bones, the orbital and intracranial widths of the OC were determined to be an average of 4.74 mm and 5.48 mm, respectively [21]. In another study conducted on 30 dry bones, the average orbital width of the OC and intracranial width were higher on the right side compared to the left [40].

In CT studies, the orbital and intracranial width of the OC were found to range between 2.9–4.6 mm and

Table 4 Comparison of optic canal measurements with some previous studies

Study	*N*	Method	Orbital width of OC	Intracranial width of OC	Medial wall length of OC	Lateral wall length of OC	ALC-OC	FZ-OC
			Mean ± SD (mm)	Mean ± SD (mm)	Mean ± SD (mm)	Mean ± SD (mm)	Mean ± SD (mm)	Mean ± SD (mm)
Radunovic et al. [40]	30	Dry skulls	L: 4.86 ± 0.70 R: 4.91 ± 0.71	L: 4.85 ± 0.49 R: 4.90 ± 0.51	13.43 ± 2.06	8.36 ± 1.83	–	–
Akdemir et al. [45]	50	Cadaver	L: 7.38 ± 2.01 R: 7.43 ± 1.95	L: 7.38 ± 2.01 R: 7.43 ± 1.95	–	–	–	–
Nitek et al. [19]	100	CT	–	–	–	–	M: 32.1 F: 32.8	M: 38.0 F: 37.4
Fetouh et al. [48]	104	Dry skulls	–	–	–	–	M: 47.25 ± 2.11 F: 46.21 ± 2.88	M: 44.25 ± 2.31 F: 43.58 ± 3.12
Gosavi et al. [22]	136	Dry skulls	–	–	–	–	L: 39.77 ± 2.63 R:39.69 ± 2.71	L: 45.61 ± 4.17 R:46.33 ± 3.71
Kalthur et al. [21]	50 214	Dry skulls CT	4.74 ± 0.47 2.98 ± 0.56	5.48 ± 0.76 4.59 ± 0.83	9.10 ± 1.46 10.63 ± 1.72	8.66 ± 1.31 9.20 ± 1.33	– –	– –
Hart et al. [20]	191	CT	4.5	6.7	14.8	10.5		
Karakas et al. [46]	62	Dry skulls	–	–	–	–	41.7 ± 3.1	44.9 ± 2.5
Huanmanop et al.[47]	100	Dry skulls	–	–	–	–	42.2 ± 2.3	46.9 ± 2.4
Celik et al. [49]	262	Dry skulls	–	–	–	–	41.4 ± 3.8	–
Pirinc et al. [42]	400	CT	R-M: 3.72 ± 0.65 L-M: 3.82 ± 0.6 R-F: 3.7 ± 0.62 L-M: 3.88 ± 0.57	R-M: 5.87 ± 1.53 L-M: 5.93 ± 1.41 R-F: 5.33 ± 1.13 L-F:5.26 ± 1.04	R-M: 10.86 ± 2.31 L-M: 10.8 ± 2.17 R-F: 10.27 ± 5 L-F: 9.4 ± 1.99	R-M: 10.59 ± 2.1 L-M: 10.02 ± 2.03 R-F: 9.5 ± 2.01 L-F: 9.24 ± 1.84	–	–
The present study	438	CT	M: 3.50 ± 1.50 F: 3.28 ± 1.54	M: 7.52 ± 1.82 F: 7.44 ± 1.91	M: 7.59 ± 3.45 F: 7.05 ± 3.35	M: 9.08 ± 2.75 F: 8.56 ± 2.67	M: 44.98 ± 4.36 F: 44.70 ± 3.75	M: 49.51 ± 3.74 F: 48.98 ± 4.45

N Number of optic canals, *M* Male, *F* Female, *R* Right, *L* Left, *OC* optic canal, *OC-FZ* distance between optic canal and frontozygomatic suture, *OC-ALC* distance between optic canal and anterior lacrimal crest, *SD*-Standard Deviation

4–6.7 mm, respectively [20, 21, 38, 41]. Some CT studies revealed wider intracranial and orbital widths of the OC in men than in women [21, 38]. Additionally, a study on 3D-CT like ours reported a significantly wider intracranial width of the OC in men than in women [42]. However, in our study, although the orbital and intracranial widths of the OC were wider in males than females, this difference was not statistically significant. This finding aligns with Hart et al. [20], who observed higher width values in males without statistical significance. Furthermore, a study noted that women with normal tension glaucoma exhibited smaller orbital aperture widths compared to men, potentially predisposing them to a higher incidence and faster progression of the disease [43].

Patients with traumatic neuropathy require knowledge of the OC length to determine the opening length [38]. The success of endoscopic optic nerve decompression may be influenced by the length of the medial canal wall [20]. In a study, it was found that the medial wall of the OC had the longest length. Instead of completely removing the medial wall during optic nerve decompression, the shortest portion of the medial wall was removed to alleviate pressure on the

nerve. This approach has been shown to minimize the risk of serious complications such as cerebrospinal fluid leakage during endoscopic endonasal procedures [44]. Radunovic et al. [40] found that the medial wall of the OC is longer than the lateral wall, measuring 13.43 ± 2.06 mm and 8.36 ± 1.83 mm, respectively. In a study employing a transsphenoidal approach, it was observed that the medial wall of the OC is the longest, and a portion of this wall is removed to alleviate compression. This approach has been shown to effectively reduce the risk of complications such as cerebrospinal fluid leakage [44]. Previous studies have shown that OC's medial and lateral wall lengths are longer in males than in females, with statistically significant differences between sides [21, 42]. Although our study found no statistical difference according to lateralization similar to Hart et al. [20], consistent with the literature, OC's lateral wall length was statistically longer in males than in females.

Morphometric measurements of the distance from the medial wall of the orbit to the OC are crucial in various surgical procedures, including ethmoid vessel ligation, investigation of medial wall fractures, anterior skull base reconstruction, tumor resection, ethmoid sinus pivot, orbital decompression, transethmoidal sphenoidotomy, and transethmoidal and sphenoidal hypophysectomy. Our study measured the distance from the OC to ALC and FZ points using 3D-CT scans. According to several studies in the literature, the average distance from the ALC point on the medial wall of the orbit to the OC ranged from 37 to 47 mm [19, 22, 45–49]. The study conducted on CT images showed that the mean distances from the OC to ALC were statistically significantly higher in men than women [50]. However, in our study, these distances were similar between genders, with no significant difference observed.

Intraorbital operations related to the lateral wall of the orbit include exploration of orbital fractures, lateral orbitotomy, and excision of the lacrimal gland. Once the periosteum is elevated, the FZ line can be detected and used as a constant landmark for this wall [47]. In previous dry skull studies, the distance between the OC and FZ has been measured to be between 45 and 47 mm [46–48]. A study employing an endoscopic surgical approach measured the safe surgical corridor distance from the FZ to the OC as 39.6 mm [17]. In the current study, the average distances between the OC and FZ were higher than other studies in the literature: 49.51 mm in males and 48.98 mm in females [19, 45–48]. These divergent results may stem from racial differences and variations in measurement methods. Additionally, considering that damage to any part of the pathway to the optic nerve can result in visual impairments, knowledge of the general characteristics of the OC and related structures is vital for surgeons approaching vascular lesions in this region.

Furthermore, tumors such as meningiomas, schwannomas, and meningiomas may grow, necessitating access to various parts of the OC. Bone removal from the OC is a standard procedure for accessing tumors and aneurysms in this area [21]. Therefore, the current study is essential in providing comprehensive data on the OC and its related structures. In this approach eliminates the need for orbital rim or frontal bone convexity removal and minimizes brain manipulation [17]. Our study aims to furnish safe surgical distances to the OC and offer extensive anatomical and morphometric information that can aid ophthalmologists and neurosurgeons in surgical planning.

The study has some limitations. Firstly, it is retrospective and includes only the Turkish population aged 18 and over. We believe it would be beneficial to include individuals under 18 and compare them with different populations to enhance the relevance of the findings. Furthermore, while there are separate studies on SOF and OC in the literature, our study contributes new data by examining the morphometric and shape relationships between these structures. Additionally, details such as SOF typing were addressed in the study. The individual analysis of all these measurements and using 3D-CT imaging set our study apart from others. To our knowledge, no other research in the literature examines these structures with a sample size as substantial as ours. We consider the data obtained from the study vital because it may contribute to updating and improving the knowledge of clinicians performing endoscopic surgery regarding the SOF and OC structures from a 3D-CT perspective.

Conclusion

Our study determined that as the SOF's width increased, the SOF's length also increased, and there was a statistically strong positive correlation. It was emphasized once again that the SOF is important in terms of area, especially in lateral edge interventions; the shape and dimensions of the fissure should be fully informed. The current study may contribute to a more effective and safer operation by improving and updating the surgeons' knowledge about the interventions from the CBW anatomical point to the SOF from the 3D-CT perspective in endoscopic procedures. Additionally, EIS-MMS, EIS-MLS, and Angle 2 parameters were measured using a different method in a previous literature study, and it was found that they were not affected by gender, sides, and age range. A narrow Angle 1 is vital for direct access to the lateral part of the SOF, and it has been found that this value is significantly smaller in males.

Furthermore, although separate studies on SOF and OC are in the literature, our study provides new data by examining the relationship between these structures' morphometric and shape relationships. Thorough knowledge of the standard dimensions of OC is essential for evaluating and managing diseases involving the canal. The present study showed that the lateral wall length of OC is affected by gender.

Author contributions Methodology, Software, Visualization, Investigation: Esin Erbek, Aynur Emine Çiçekcibaşı, Betül Digilli Ayaş, Gülay Açar, Demet Aydoğdu. Data curation, Original draft preparation: Esin Erbek, Aynur Emine Çiçekcibaşı, Demet Aydoğdu.Validation, Supervision: Esin Erbek, Aynur Emine Çiçekcibaşı, Gülay Açar. Figures and tables preparation: Esin Erbek, Betül Digilli Ayaş.Writing and Reviewing: Esin Erbek, Aynur Emine Çiçekcibaşı, Betül Digilli Ayaş, Gülay Açar.

Funding No funds, grants, or other support were received.

Data availability The data supporting this study's findings are available from the corresponding author upon reasonable request.

Declarations

Conflict of interest The authors have no relevant financial or non-financial interests to disclose.

Ethical approval This study was performed in line with the principles of the Declaration of Helsinki. Approval was granted by the Ethics Committee of Necmettin Erbakan University (approval number, 2021/3391).

References

1. Abed SF, Shams P, Shen S et al (2011) A cadaveric study of the morphometric and geometric relationships of the orbital apex. Orbit 30:72–76. https://doi.org/10.3109/01676830.2010.538126
2. Engin O, Adriaensen GFJPM, Hoefnagels FWA, Saeed P (2021) A systematic review of the surgical anatomy of the orbital apex. Surg Radiol Anat 43:169–178. https://doi.org/10.1007/s00276-020-02573-w
3. La Marra A, Quarchioni S, Ferrari F et al (2016) 640-Slice CT measurement of superior orbital fissure as gateway for light into the brain: statistical evaluation of area and distance. PLoS ONE 11:e0162940. https://doi.org/10.1371/journal.pone.0162940
4. Standring S (2008) Gray's anatomy: the anatomical basis of clinical practice Forty-first ed. Elsevier Health Sciences, London
5. Kumar A, Tripathi A, Jain S et al (2019) Anatomical and morphometric study of optic foramen in North Indian population. Natl J Clin Anat 8:53–56. https://doi.org/10.1055/s-0039-1689079
6. Abuzayed B, Tanriover N, Gazioglu N et al (2009) Endoscopic endonasal approach to the orbital apex and medial orbital wall: anatomic study and clinical applications. J Craniofac Surg 20:1594–1600. https://doi.org/10.1097/SCS.0b013e3181b0dc23
7. Li L, London NR, Chen X et al (2020) Expanded exposure and detailed anatomic analysis of the superior orbital fissure: implications for endonasal and transorbital approaches. Head Neck 42:3089–3097. https://doi.org/10.1002/hed.26399
8. Martins C, Costa E Silva IE, Campero A et al (2011) Microsurgical anatomy of the orbit: the rule of seven. Anat Res Int 2011:1–14. https://doi.org/10.1155/2011/468727
9. Gonul E, Erdogan E, Duz B, Timurkaynak E (2003) Transmaxillary approach to the orbit: an anatomic study. Neurosurgery 53:935–942. https://doi.org/10.1227/01.NEU.0000084164.22028.10
10. Ong BC, Gore PA, Donnellan MB et al (2008) Endoscopic sublabial transmaxillary approach to the rostral middle fossa. Neurosurgery 62(3):30–37. https://doi.org/10.1227/01.neu.0000317371.92393.33
11. Schultheiß S, Petridis AK, El Habony R et al (2013) The transmaxillary endoscopic approach to the orbit. Acta Neurochir (Wien) 155:87–97. https://doi.org/10.1007/s00701-012-1525-8
12. Wang X, Li YM, Huang CG et al (2014) Endoscopic transmaxillary transMüller's muscle approach for decompression of superior orbital fissure: a cadaveric study with illustrative case. J Craniomaxillofac Surg 42:132–140. https://doi.org/10.1016/j.jcms.2013.03.008
13. Otani N, Wada K, Fujii K et al (2016) Usefulness of extradural optic nerve decompression via trans–superior orbital fissure approach for treatment of traumatic optic nerve injury: surgical procedures and techniques from experience with 8 consecutive patients. World Neurosurg 90:357–363. https://doi.org/10.1016/j.wneu.2016.03.013

14. Ulutas M, Boyacı S, Akakın A et al (2016) Surgical anatomy of the cavernous sinus, superior orbital fissure, and orbital apex via a lateral orbitotomy approach: a cadaveric anatomical study. Acta Neurochir (Wien) 158:2135–2148. https://doi.org/10.1007/s00701-016-2940-z
15. Shi X, Han H, Zhao J, Zhou C (2007) Microsurgical anatomy of the superior orbital fissure. Clin Anat 20:362–366. https://doi.org/10.1002/ca.20391
16. Dallan I, Castelnuovo P, De Notaris M et al (2013) Endoscopic endonasal anatomy of superior orbital fissure and orbital apex regions: critical considerations for clinical applications. Eur Arch Otorhinolaryngol 270:1643–1649. https://doi.org/10.1007/s00405-012-2281-3
17. Di Somma A, Cavallo LM, De Notaris M et al (2017) Endoscopic endonasal medial-to-lateral and transorbital lateral-to-medial optic nerve decompression: an anatomical study with surgical implications. J Neurosurg 127:199–208. https://doi.org/10.3171/2016.8.JNS16566
18. Reymond J, Kwiatkowski J, Wysocki J (2008) Clinical anatomy of the superior orbital fissure and the orbital apex. J Craniomaxillofac Surg 36:346–353. https://doi.org/10.1016/j.jcms.2008.02.004
19. Nitek S, Bakoń L, Sharifi M et al (2015) Morphometry of the orbit in East-European population based on three-dimensional CT reconstruction. Adv Anat 2015:1–10. https://doi.org/10.1155/2015/101438
20. Hart CK, Theodosopoulos PV, Zimmer LA (2009) Anatomy of the optic canal: a computed tomography study of endoscopic nerve decompression. Ann Otol Rhinol Laryngol 118:839–844. https://doi.org/10.1177/000348940911801203
21. Kalthur S, Periyasamy R, Kumar S et al (2015) A morphometric evaluation of the optic canal: comparative study between computerized tomographic study and direct anatomic study. Saudi J Med Med Sci 3:204–208
22. Gosavi SN, Jadhav SD, Zambare BR (2014) Orbital morphology with reference to bony landmarks. Rev Arg de Anat Clin 6:20–25. https://doi.org/10.31051/1852.8023.v6.n1.14094
23. Park Y, Kim Y (2017) A statistical analysis of superior orbital fissure width in korean adults using computed tomography scans. Arch Craniofac Surg 18:89–91. https://doi.org/10.7181/acfs.2017.18.2.89
24. Hu S, Colley P (2019) Surgical orbital anatomy. Semin Plast Surg 33:085–091. https://doi.org/10.1055/s-0039-1685476
25. Beriat GK, Atac GK, Kocaturk S et al (2013) A simple technique for removal of orbital tumors: transmaxillary approach. Tr-ENT 23:299–301. https://doi.org/10.5606/kbbihtisas.2013.16779
26. Fujiwara T, Matsuda K, Kubo T et al (2009) Superior orbital fissure syndrome after repair of maxillary and naso-orbito-ethmoid fractures: a case study. JPRAS 62:e565–e569. https://doi.org/10.1016/j.bjps.2008.11.052
27. Govsa F, Kayalioglu G, Erturk M, Ozgur T (1999) The superior orbital fissure and its contents. Surg Radiol Anat 21:181. https://doi.org/10.1007/bf01630898
28. Ozcan SC, Onder F, Demir N, Ozcan DO (2019) Traumatic superior orbital fissure syndrome. GMS Ophthalmol Cases. https://doi.org/10.3205/oc000099
29. Sirikonda P, Katikireddi R, Vedapriya K (2022) Morphology and morphometric study of superior orbital fissure in dried human skulls. IJARS. https://doi.org/10.7860/ijars/2022/47282.2740
30. Natori Y, Rhoton AL (1994) Transcranial approach to the orbit: microsurgical anatomy. J Neurosurg 81:78–86. https://doi.org/10.3171/jns.1994.81.1.0078
31. Pirinc B, Fazliogullari Z, Koplay M et al (2023) Morphometric evaluation and classification of the superior orbital fissure on 3D MDCT images. Anat Sci Int 98:196–203. https://doi.org/10.1007/s12565-022-00687-2
32. Kaur A, Delmotra P, Singh K et al (2022) Morphometric dimensions of superior orbital fissure: a cross-sectional study. IJARS 11:AO26–AO28. https://doi.org/10.7860/IJARS/2022/47686.2808
33. Patel AK, Tripathi A, Kumar R, Patel RB (2021) Anatomical and radiological study of superior orbital fissure. Maedica 16:599–602
34. Sharma PK, Malhotra VK, Tewari SP (1988) Variations in the shape of the superior orbital fissure. Anat Anz 165:55–56
35. Magden AO, Kaynak S (1996) Bilateral duplication of the optic canals. Ann Anat 178:61–64. https://doi.org/10.1016/s0940-9602(96)80013-6
36. Dande K, Archana R, Verma RK, Sharma PK (2022) Morphological and morphometric variation of superior orbital fissure. IJARS 11:AO40–AO43. https://doi.org/10.7860/IJARS/2022/47282.2740
37. Purohit BJ, Singh PR (2016) An osteologic study of cranial opening of optic canal in gujarat region. J Clin Diagn Res 10:AC08-AC11. https://doi.org/10.7860/JCDR/2016/22110.8929
38. Sthapak E, Pasricha N, Narayan S et al (2023) Optic canal: a CT-based morphometric study in North Indian population. Egypt J Neurosurg 38:46. https://doi.org/10.1186/s41984-023-00220-1
39. Sinanoglu A, Orhan K, Kursun S et al (2016) Evaluation of optic canal and surrounding structures using cone beam computed tomography: considerations for maxillofacial surgery. J Craniofac Surg 27:1327–1330. https://doi.org/10.1097/SCS.0000000000002726
40. Radunovic M, Vukcevic B, Radojevic N et al (2019) Morphometric characteristics of the optic canal and the optic nerve. Folia Morphol 78:39–46. https://doi.org/10.5603/fm.a2018.0065
41. Liu J, Zhao J, Wang Y et al (2022) Simultaneous endoscopic endonasal decompression of the optic canal, superior orbital fissure, and proper orbital apex for traumatic orbital apex syndrome: surgical anatomy and technical note. Front Surg 8:811706. https://doi.org/10.3389/fsurg.2021.811706
42. Pirinc B, Fazliogullari Z, Koplay M et al (2023) Morphometric and morphological evaluation of the optic canal in three different parts in MDCT images. Int Ophthalmol 43:2703–2720. https://doi.org/10.1007/s10792-023-02670-w
43. Pircher A, Montali M, Berberat J et al (2017) The optic canal: A bottleneck for cerebrospinal fluid dynamics in normal-tension glaucoma? Front Neurol 8:47. https://doi.org/10.3389/fneur.2017.00047

44. Li J, Ran QS, Hao B, Xu X et al (2020) Transsphenoidal optic canal decompression for traumatic optic neuropathy assisted by a computed tomography image postprocessing technique. J Ophthalmol 2020:1870745. https://doi.org/10.1155/2020/1870745
45. Akdemir G, Tekdemir I, Altın L (2004) Transethmoidal approach to the optic canal: surgical and radiological microanatomy. Surg Neurol 62:268–274. https://doi.org/10.1016/j.surneu.2004.01.022
46. Karakas P, Bozkır M, Oguz O (2002) Morphometric measurements from various reference points in the orbit of male Caucasians. Surg Radiol Anat 24:358–362. https://doi.org/10.1007/s00276-002-0071-0
47. Huanmanop T, Agthong S, Chentanez V (2007) Surgical anatomy of fissures and foramina in the orbits of thai adults. J Med Assoc Thai 90:2383–3239
48. Fetouh FA, Mandour D (2014) Morphometric analysis of the orbit in adult Egyptian skulls and its surgical relevance. Eur J Anat 18:303–315
49. Celik S, Ozer MA, Kazak Z, Govsa F (2015) Computer-assisted analysis of anatomical relationships of the ethmoidal foramina and optic canal along the medial orbital wall. Eur Arch Otorhinolaryngol 272:3483–3490. https://doi.org/10.1007/s00405-014-3378-750
50. Singh J, Ab Rahman R, Rajion ZA et al (2017) Orbital morphometry: a computed tomography analysis. J Craniofac Surg 28:e64–e70. https://doi.org/10.1097/scs.0000000000003218